.

Effect of dopant concentration and excitation intensity on the upconversion and downconversion emission of β-$NaYF_4$:Yb^{3+},Er^{3+} nanoparticles

Electronic Supplementary Information (ESI)

Vivian Torres Vera,[a] Diego Mendez-Gonzalez,[a] Diego J. Ramos-Ramos,[b,c] Asmae Igalla,[b] Marco Laurenti,[a] Rafael Contreras-Caceres,[a] Enrique Lopez-Cabarcos,[a] Elena Díaz,[c] Jorge Rubio-Retama,[a] Sonia Melle,[b] and Oscar G. Calderón*[b]

Contents

S1. EDS measurements: estimation of Yb^{3+}/Er^{3+} dopant ratios.

S2. TEM images showing nanoparticle size histograms for UCNPs with different Yb^{3+}/Er^{3+} ratios.

S3. XRD measurements: crystalline phase for UCNPS with different Yb^{3+}/Er^{3+} ratios.

S4. Parameter values used in the theoretical model

S5. Derivation of the analytical expression for the population of the excited states in the low excitation signal regime

[a] *Department of Chemistry in Pharmaceutical Sciences, Complutense University of Madrid, E-28040 Madrid, Spain*
[b] *Department of Optics, Complutense University of Madrid, E-28037 Madrid, Spain. E-mail: oscargc@ucm.es*
[c] *GISC, Department of Materials Physics, Complutense University of Madrid, E-28040 Madrid, Spain*

S1. EDS measurements: estimation of Yb^{3+}/Er^{3+} dopant ratios.

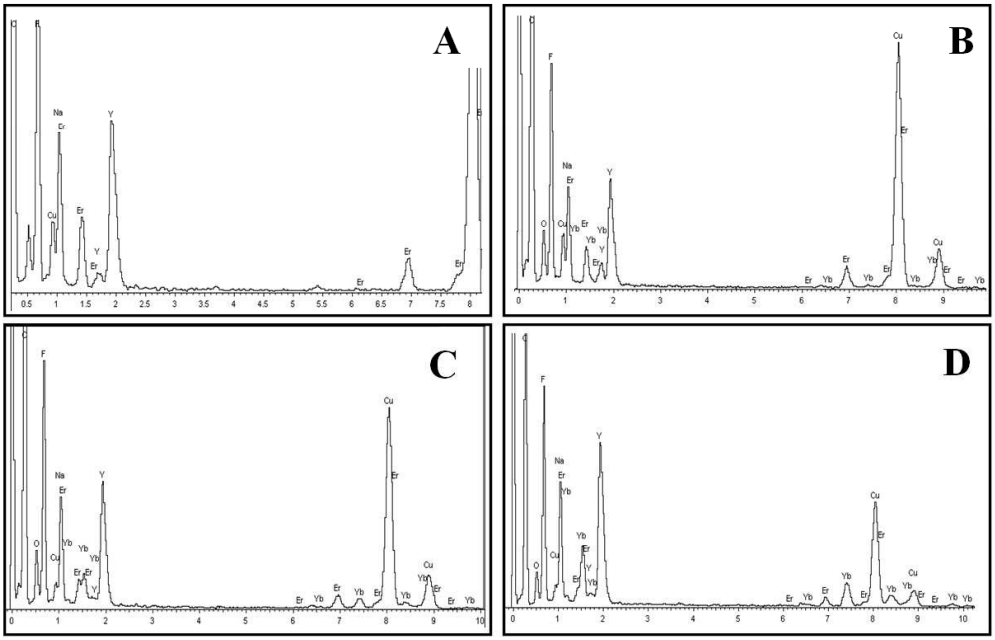

E

Nominal Yb^{3+}/Er^{3+}	at % Y^{3+}	at % Yb^{3+}	at % Er^{3+}	Yb^{3+}/Er^{3+} from EDS
0	80.23	0.00	19.77	0
0.1	76.65	1.71	21.64	0.08
0.25	77.25	4.55	18.20	0.25
1	80.14	10.77	9.09	1.2

Fig. S1. (A-D) EDS spectrum for $NaYF_4$:Er^{3+},Yb^{3+} nanoparticles with representative Yb^{3+}/Er^{3+} dopant ratios: (A) Ratio 0. (B) Ratio 0.1. (C) Ratio 1. (D) Ratio 4. (E) Table including the atomic percent of lanthanides present into the nanoparticle unit cell obtained from EDS analysis.

S2. TEM images showing nanoparticle size histograms for UCNPs with different Yb^{3+}/Er^{3+} ratios.

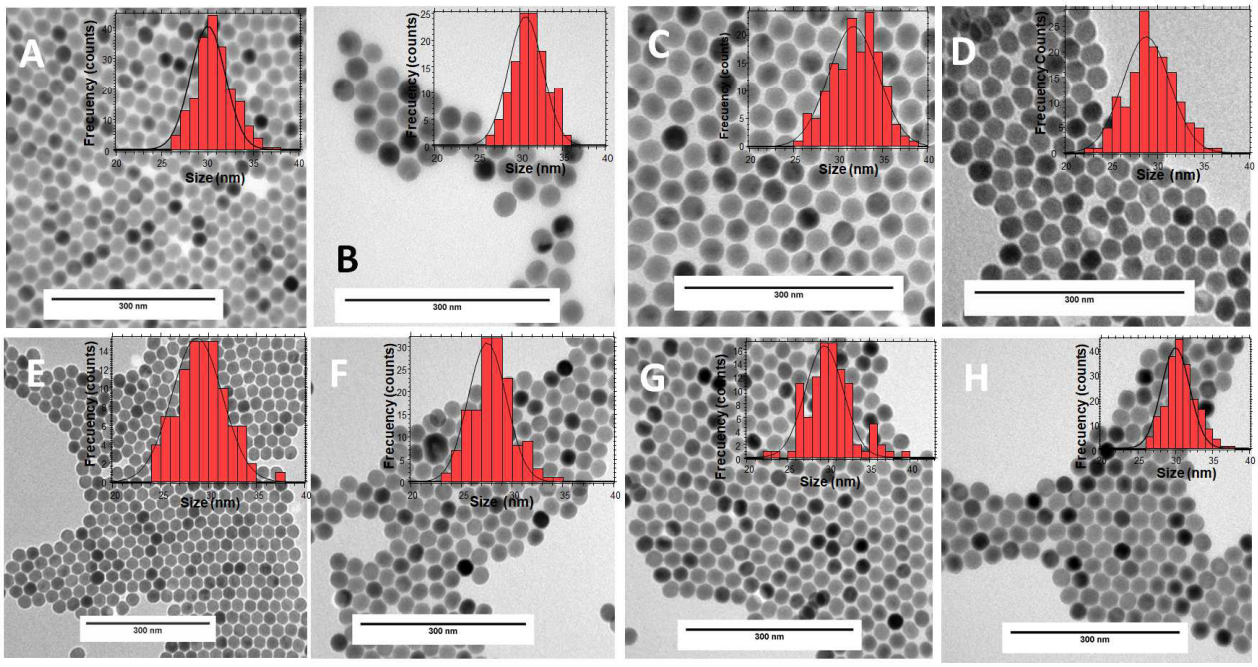

Fig. S2. TEM sizes for different Yb/Er ratios: (A) Ratio 10. (B) Ratio 8. (C) Ratio 4. (D) Ratio 1. (E) Ratio 0.25. (F) Ratio 0.12. (G) Ratio 0.1. (H) Ratio 0.

S3. XRD measurements: crystalline phase for UCNPS with different Yb^{3+}/Er^{3+} ratios.

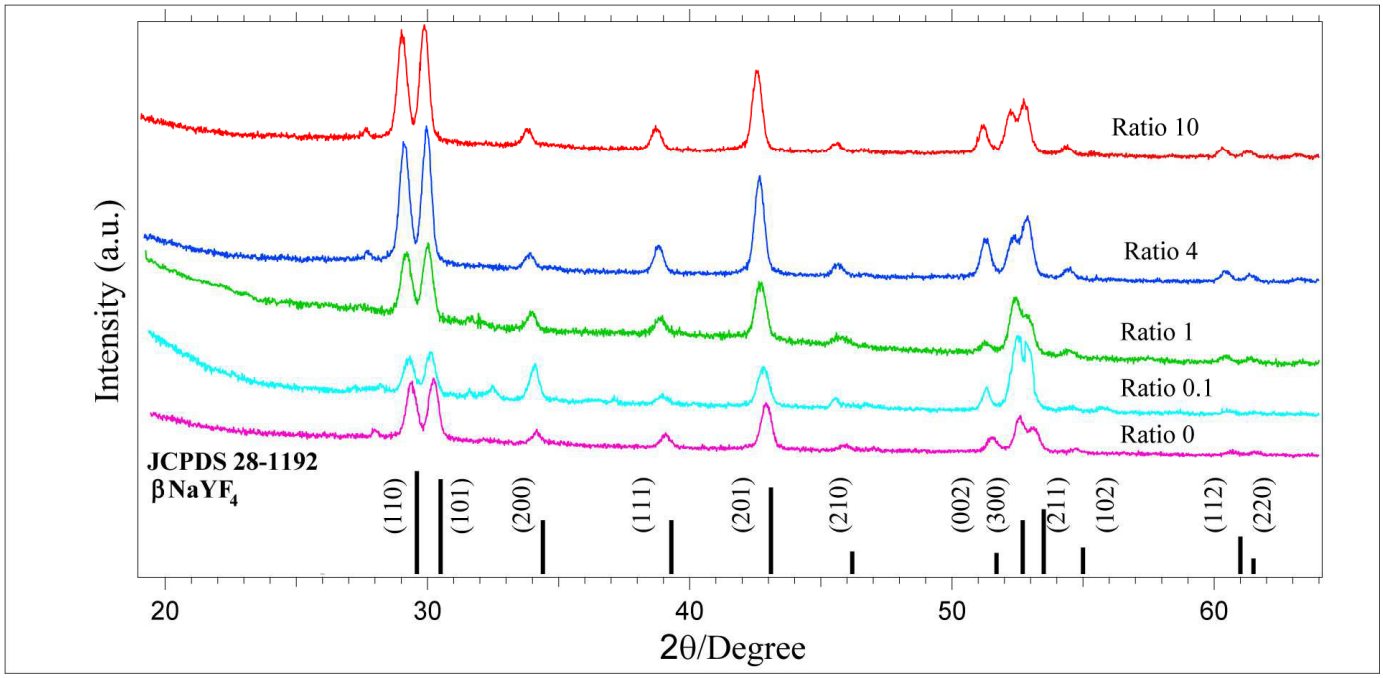

Fig. S3. XRD pattern for different Yb/Er ratios in agreement with the literature reference for β-$NaYF_4$ crystal (Joint Committee on Powder Diffraction Standards file number 28-1192)

S4. Parameter values used in the theoretical model.

The parameter values used in the theoretical model are similar to those found in literature[1–4]. Moreover, some of them were used as control parameters to correctly reproduce the experimental results. Er^{3+} ions in the metastable level 1 ($^4I_{13/2}$) (see Fig. 6) radiatively decay to the ground state $^4I_{15/2}$ with a decay time of $1/W_1 = 4$ ms while Yb^{3+} ions in level 1 (see Fig. 6) decay to the ground state with a decay time of $1/W_1^Y = 2$ ms. The other energy levels of Er^{3+} ions present two contributions, a radiative decay rate to the ground state in the millisecond range ($1/W_{20} = 2$ ms, $1/W_{30} = 1$ ms, and $1/W_{40} = 1$ ms) and a faster nonradiative decay rate to the next lower level (partially due to multi-phonon relaxation) which is within the microsecond range. Here, we used an intrinsic quantum yield for the green level 4 (see Fig. 6), $\eta_0 = W_{40}/(W_{40} + W_{43}) \simeq 0.06$, which leads to $W_{43} = 1.6 \times 10^4$ s^{-1}. For simplicity, we took the same value for the rest of nonradiative decay rates, $W_{32} = W_{21} = W_{43}$ (see Fig. 6). Furthermore, the following values for the resonant energy transfer parameters are considered. Concerning the energy transfer from Yb^{3+} to Er^{3+} ion (see Fig. 6), we set $K_2 = 5 \times 10^{-17}$ cm^3 s^{-1}, a similar value for the back energy transfer $K_{B2} = K_2$, and a lower value for $K_4 = 0.5K_2$. Taking into account our experimental results that indicate that both UCL emission bands have the same behavior with the Yb/Er ratio, we assume that the main population pathway for the red-emitting level is through the green-emitting level. Therefore, we neglected in the simulations the energy transfer from level $^4I_{13/2}$ ($K_3 = 0$) and also the excited state absorption from this level ($\sigma_{13} = 0$) (see Fig. 6). The energy transfer coefficients between neighbors Er^{3+} ions (see Fig. 6) were taken $C_1 = 1.2 \times 10^{-17}$ cm^3 s^{-1} and $C_2 = 1.8 \times 10^{-17}$ cm^3 s^{-1}. The absorption cross-section of the Yb^{3+} transition $\sigma^Y = 1.7 \times 10^{-20}$ cm^2 is much larger than the corresponding to the Er^{3+} transition $\sigma_{02} = 0.68 \times 10^{-21}$ cm^2. The excited state transition from level $^4I_{11/2}$ to the green-emitting level (see Fig. 6) is similar to the previous one, i.e, $\sigma_{24} = \sigma_{02}$. With these values, we obtained a saturation intensity of $I_{sat}^Y = 3$ kW/cm^2 for the Yb^{3+} transition and a much larger saturation value for the corresponding Er^{3+} transition $I_{sat} = 75$ kW/cm^2. For the range of excitation laser powers used in our experiments, we operate below and above the saturation value of Yb^{3+} transition but very far away from the saturation value of Er^{3+} transition. Therefore, the behavior of the luminescence with the laser power is expected to be different for very low Yb/Er ratios (absorption of Er^{3+} ions without saturation) than for high ones (absorption of Yb^{3+} ions with possible saturation). To numerically study the effect of the Yb/Er ratio in the luminescence of the UCNPs, we varied the concentration of Er^{3+} and Yb^{3+} dopants accordingly with the Yb/Er ratios. To estimate the concentration of Er^{3+} (N_{Er}) and Yb^{3+} (N_{Yb}) ions, we followed the molecular weight calculation of UCNPs by Mackenzie et al.[5] We used the hexagonal crystal lattice parameters $a_h = 0.596$ nm and $c_h = 0.353$ nm to calculate the volume of a unit cell in the UCNP ($u_V \simeq 0.1086$ nm^3). Then, we took into account the fractional percentage of RE dopants f_{RE} ($RE = Yb$ and Er) to compute the RE ion concentration $N_{RE} = 1.5 f_{RE}/u_V$. We solved Equation 1 using an explicit Runge-Kutta method in MatLab[6] considering that all population is initially in the ground states ($N_0 = N_{Er}$ and $N_0^Y = N_{Yb}$). After an initial transient, the system reached the steady-state, and the final populations allowed us to compute the luminescence intensity.

S5. Derivation of the analytical expression for the population of the excited states in the low excitation signal regime

We analytically solved the rate equation model (Equation 1 in Sec. 3.3) in the steady state (time derivatives set to zero) by considering the small excitation signal regime, i.e., $I/I_{sat}^{Y} \ll 1$. In this case, most of the population remains in the ground state ($N_0 \simeq N_{Er}$ and $N_0^Y \simeq N_{Yb}$) and the population of the excited states are obtained linearizing the Equation 1 in Sec. 3.3 as follows:

$$
\begin{aligned}
0 &= -W_1 N_1 + W_{21} N_2 \ , \\
0 &= -W_2 N_2 + K_2 N_{Er} N_1^Y - K_{B2} N_{Yb} N_2 + \frac{W_1 I}{I_{sat}} N_{Er} \ , \\
0 &= -W_3 N_3 + W_{43} N_4 \ , \\
0 &= -W_4 N_4 + K_4 N_2 N_1^Y + C_2 N_2^2 \ , \\
0 &= -W_1^Y N_1^Y + \frac{W_1^Y I}{2 I_{sat}^Y} N_{Yb} - K_2 N_{Er} N_1^Y + K_{B2} N_{Yb} N_2 \ ,
\end{aligned}
\qquad (S1)
$$

where N_1^Y, N_1 and N_2 are first-order perturbations and N_3 and N_4 are second-order perturbations in the excitation intensity respectively. We have not included the processes neglected in our simulations ($K_3 = 0$ and $\sigma_{13} = 0$, see Sec. S4 in ESI) and the contribution of ESA ($\sigma_{24} = 0$) which has been found to be negligible in comparison with Er-Er-ETU (see Figure 7A). From the above linear system of equations (Equation S1) we obtained the analytical steady state populations:

$$
\begin{aligned}
N_1^Y &= \frac{\frac{W_1^Y N_{Yb}}{W_1^Y + K_2 N_{Er}} \frac{I}{2 I_{sat}^Y} + \frac{W_1 K_{B2} N_{Yb} N_{Er}}{(W_1^Y + K_2 N_{Er})(W_2 + K_{B2} N_{Yb})} \frac{I}{I_{sat}}}{1 - \frac{K_2 K_{B2} N_{Yb} N_{Er}}{(W_1^Y + K_2 N_{Er})(W_2 + K_{B2} N_{Yb})}} \ , \\
N_2 &= \frac{K_2 N_{Er}}{W_2 + K_{B2} N_{Yb}} N_1^Y + \frac{W_1 N_{Er}}{W_2 + K_{B2} N_{Yb}} \frac{I}{I_{sat}} \ , \\
N_1 &= \frac{W_{21}}{W_1} N_2 \ , \\
N_4 &= \frac{K_4}{W_4} N_2 N_1^Y + \frac{C_2}{W_4} N_2^2 \ , \\
N_3 &= \frac{W_{43}}{W_3} N_4 \ .
\end{aligned}
\qquad (S2)
$$

These analytical expressions (Equation S2) allow us to theoretically analyze the UCL and DCL emission intensity. In Figure S5 we compare the analytical populations given by Equation S2 (colored solid lines) with the result obtained by numerically solving Equation 1 in Sec. 3.3 (colored open circles) in the case of low excitation intensities ($I/I_{sat}^{Y} = 0.001$). A perfect agreement is observed. Furthermore, we also plotted (black solid lines) the experimental power law obtained for the DCL and UCL intensities with the Yb/Er ratio (exponent 0.6 for DCL and 1.4 for UCL from Figure 3B and 3D). Both, the numerical simulations and the analytical result from Equation S2, nicely match with the experimental behavior.

With the aim of obtaining a very simple and direct expression for the populations N_1 and N_4 as a function of the Yb/Er ratio we further simplified Equation S2. We first simplified the population of the Yb^{3+} excited state $^2F_{5/2}$, N_1^Y in Equation S2, by taking into account that $W_1^Y + K_2 N_{Er} \simeq K_2 N_{Er}$ and that the second term of the right hand side of N_1^Y is smaller than the first term since $(W_2 + K_{B2} N_{Yb})/(K_{B2} N_{Er}) > \sigma_{02}/\sigma^Y$. Then, we simplified N_2 in Equation S2 by keeping only the first term of the right hand side, which is larger than the second one while $N_{Yb}/N_{Er} > (\sigma_{02}/\sigma^Y) W_2/(W_2 + K_{B2} N_{Yb})$, which takes place in most of the analyzed ratios. Therefore, the population equations remain:

$$
\begin{aligned}
N_1^Y &= \frac{W_1^Y (W_2 + K_{B2} N_{Yb}) N_{Yb}}{W_2 K_2 N_{Er}} \, \frac{I}{2 I_{sat}^Y} \, , \\
N_2 &= \frac{W_1^Y N_{Yb}}{W_2} \, \frac{I}{2 I_{sat}^Y} \, , \\
N_1 &= \frac{W_{21}}{W_1} N_2 \, , \\
N_4 &= \frac{1}{W_4} \left(\frac{W_1^Y}{W_2} \right)^2 N_{Yb}^2 \left[\frac{K_4}{K_2} \, \frac{W_2 + K_{B2} N_{Yb}}{N_{Er}} + C_2 \right] \left(\frac{I}{2 I_{sat}^Y} \right)^2 \, , \\
N_3 &= \frac{W_{43}}{W_3} N_4 \, .
\end{aligned}
\qquad (S3)
$$

We also plotted in Figure S5 the analytical populations given by Equation S3 (colored dashed lines), which still show a good agreement with the numerical simulations. More interestingly, these analytical population equations allowed us to nicely reproduce the enhancement of the DCL and UCL intensity found in the experiments. In particular, the best agreement between Equation S3 and the experimental power law behavior is found for ratios within the intermediate range $[0.2 - 1.0]$ (see Figure S5). Therefore, we can analytically write simple dependencies for the populations N_1 and N_4 on the Yb/Er ratio (referred as to r) valid within this range:

$$
\begin{aligned}
N_1 &= \frac{W_{21} W_1^Y}{W_1 W_2} \, N_{Yb} \, \frac{I}{2 I_{sat}^Y} \sim N_{Yb} \sim \frac{r}{1 + r} \, , \\
N_4 &= \frac{C_2}{W_4} \left(\frac{W_1^Y}{W_2} \right)^2 N_{Yb}^2 \left(\frac{I}{2 I_{sat}^Y} \right)^2 \sim N_{Yb}^2 \sim \left(\frac{r}{1 + r} \right)^2 \, .
\end{aligned}
\qquad (S4)
$$

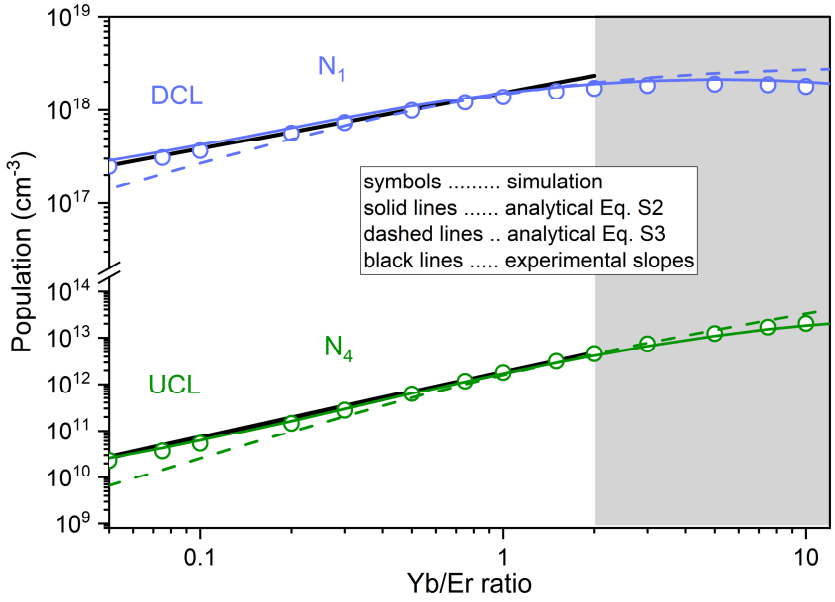

Fig. S5. Steady state populations for the green (N_4) and NIR (N_1) emission levels as a function of the Yb/Er ratio. Analytical results using Equation S2 (colored solid lines) and Equation S3 (colored dashed lines). The numerically simulated result using Equation 1 in Sec. 3.3 (symbols). Black solid lines are power laws corresponding to the fitting of the experimental data: exponent 0.6 for DCL and 1.4 for UCL.

References

1 R. B. Anderson, S. J. Smith, P. S. May and M. T. Berry, *The Journal of Physical Chemistry Letters*, 2014, **5**, 36–42.

2 N. U. Wetter, A. M. Deana, I. M. Ranieri, L. Gomes and S. L. Baldochi, *IEEE Journal of Quantum Electronics*, 2010, **46**, 99–104.

3 S. Fischer, H. Steinkemper, P. Löper, M. Hermle and J. C. Goldschmidt, *Journal of Applied Physics*, 2012, **111**, 013109.

4 M. Kaiser, C. Würth, M. Kraft, T. Soukka and U. Resch-Genger, *Nano Research*, 2019, **12**, 1871–1879.

5 L. E. Mackenzie, J. A. Goode, A. Vakurov, P. P. Nampi, S. Saha, G. Jose and P. A. Millner, *Scientific Reports*, 2018, **8**, 1106.

6 J. Dormand and P. Prince, *Journal of Computational and Applied Mathematics*, 1980, **6**, 19 – 26.